ULTRA-HIGH ENERGY COSMIC RAYS*

A.A. Watson

Department of Physics and Astronomy, University of Leeds
Leeds, LS2 9JT, UK
a.a.watson@leeds.ac.uk

(Received October 28, 2019)

The first part of this article, based on lectures given at the Cracow School of Theoretical Physics held in Zakopane in June 2019, is devoted to a brief exposition of the physics associated with the development of extensive air showers. The latter parts deal with methods of detection of extensive air showers in a general way, and include a description of the latest measurements of the energy spectrum, the arrival direction distribution and the mass composition of cosmic rays of energy above 10^{18} eV made, primarily, with the Pierre Auger Observatory. There is a brief discussion of future projects.

DOI:10.5506/APhysPolB.50.2035

1. An introduction to cosmic rays

Cosmic rays were discovered by the Austrian physicist, and enthusiastic amateur balloonist, Victor Hess, as a result of flying ionisation detectors in a series of manned balloon flights. In 1912, he ascended to over 5300 m and found that the rate of discharge of his ionisation chambers increased rapidly with altitude beyond the first kilometre above the ground. He interpreted this observation as evidence that the earth was being continuously bombarded by radiation that could cause ionisation. The story of the early years of the study of this radiation has been told many times and will be recounted only briefly here. The early workers (and notably R.A. Millikan) supposed that the extra-terrestrial radiations were gamma rays as these were the most penetrating radiations then known. It was Millikan who coined the name 'cosmic rays', using it first in a lecture to the British Association at the University of Leeds in 1926. It turns out, however, that only a small fraction

* Presented at the LIX Cracow School of Theoretical Physics "Probing the Violent Universe with Multimessenger Eyes: Gravitational Waves, High-energy Neutrinos, Gamma Rays, and Cosmic Rays", Zakopane, Poland, June 14–22, 2019.

of the radiation that causes the type of effect observed by Hess are gamma rays: in fact, most of the incoming cosmic rays are the nuclei of atoms (from hydrogen to uranium) accelerated in places in the Universe that we have yet to fully identify. Thus, the name is not very accurate.

That most of the incoming radiation consisted of charged particles was first established by Clay who collected measurements of the intensity of ionisation as a function of geomagnetic latitude on voyages between Amsterdam and the Dutch East Indies. He found that the intensity fell by about 15% between the geomagnetic latitude of Amsterdam and the geomagnetic equator. From this set of observations, confirmed through measurements made by Leprince–Ringuet and Auger on a voyage from Europe to Buenos Aires, and through a very extensive survey carried out by A.H. Compton, it was demonstrated that the major part of the radiation causing the effects observed at sea level were charged particles. The interpretation was much helped by calculations of the trajectory of charged particles in the geomagnetic fields, most notably by Stoermer in Europe and Vallarta in Mexico. Electrons were tentatively identified as the likely primary particles.

Again, as with the initial idea that the incoming radiation was primarily gamma rays, this proved to be an erroneous deduction. The experiments that clinched the issue of the charge were carried out, at the invitation of Vallarta, in Mexico City by Johnson and by Compton and Alvarez in 1933. It had been recognised, originally by Rossi, that the sign of the charge of the particles, if one charge dominated, would be reflected in the ratio of the fluxes coming from easterly and westerly directions. These definitive experiments showed that there was an excess of particles from the west, implying that the majority of particles were positively charged. The positron had been discovered in 1932 so that there was a suspicion that the cosmic rays might be positive electrons. However, in 1941, using relatively sophisticated counter systems flown in balloons, Schein and collaborators demonstrated that the bulk of the particles were probably protons. The gamma-ray and electron trails had proved to be false ones.

The direct determination of the charge spectrum of cosmic rays had to await the development of the nuclear emulsion technique with which it was established, again using balloons, that the nuclei of elements from hydrogen to iron were all present in the primary cosmic rays. The striking excesses of Li, Be and B above their normal abundances led to the conclusion that the bulk of the particles had travelled through an average of 4 $\mathrm{g\,cm^{-2}}$ of interstellar hydrogen. Subsequently, a flux of electrons was detected at an intensity of $\sim 1\%$ of the charged particle flux.

Much later, the presence of primary gamma rays was established but at an intensity of only $\sim 10^{-4}$ of the nuclear flux. Studies of great sensitivity have been made of gamma rays over a range of energies in the decades since

their discovery. Perhaps those of $\sim$ 100 MeV or so provide the strongest clues below 10^{15} eV but the question of the origin of even the lowest-energy cosmic rays is still far from settled.

A different approach to the search for the origin of cosmic rays above $\sim 10^{14}$ eV, and the one that is central to the discussions that follow, is based on the phenomenon of extensive air showers, first studied by Schmeiser and Bothe in 1937 and by Kolhörster and colleagues during the following year. These workers made targeted searches for what they called 'Luftschauer'. Their idea that such showers could exist was based on an examination of the famous Rossi transition curves and the observation of a maximum in the rate of ionisation high in the atmosphere by Regener and Pfotzer. The discovery of extensive air showers is often attributed to Pierre Auger and his collaborators in 1938 but, although he was later able to study the phenomenon in greater detail than others, Auger's first observations were, in fact, serendipitous and were made during tests of improvements to coincidence circuits developed by Roland Maze, who had designed a circuit with a resolving time of 10 μs. Auger and his group used the newly discovered concepts of quantum electrodynamics to show that coincidences seen between counters place 300 m apart could have been initiated by a photon of $\sim 10^{15}$ eV. In fact, Rossi, while working in Eritrea in 1934, had observed the phenomenon first, again serendipitously, but was unable to take his studies further because of political issues in Italy. The history of the development of extensive air showers is discussed in [1].

Study of the shower phenomenon was pursued to establish the highest energies carried by cosmic rays and also in the expectation that, at a sufficiently high energy, even charged particles would cut through the magnetic fields in interstellar and intergalactic space, and retain a memory of their starting direction when they were detected at earth. There was virtually no theoretical guidance as to what might be expected. Work progressed only slowly until the MIT group, headed by Rossi, developed a method of measuring the relative arrival times of the shower particles at dispersed detectors. In pioneering work, it was shown that an array of scintillation detectors could be used to measure the shower direction and the time spread of the particles in the shower disc. The direction of the incoming primary cosmic ray, assumed to be perpendicular to this disc, could be found with a precision of $\sim 3^\circ$.

2. The development of extensive air showers

I will now try to explain how an air shower develops. It is important to have a good and intuitive grasp of a few important quantities that define the development of the cascade and to learn how to visualise what is going

on. This is a key step to take before using, or developing, sophisticated Monte Carlo calculations that are increasingly necessary to interpret shower observations.

Two cloud-chamber photographs are shown in Fig. 1. That on the left shows a high-energy particle (probably a proton judging from the density of ionisation along the track) interacting with a nucleus of argon in a cloud chamber operated at 70 atmospheres by G.R. Evans on Mt Marmolada in the Dolomites (3343 m). Short thick tracks are probably fragments of the nucleus, while the thinner tracks are mainly of charged pions. In the right-hand photograph, taken by W.B. Fretter in a multi-plate cloud chamber at Echo Lake (3230 m), the development of a cascade shower is shown. An interaction of the type shown in the photograph on the left will have taken place in the 7^{th} lead plate: each lead plate was 1.3 cm thick. The cascade develops largely in the two radiation lengths of material in each plate: the cloud chamber enables the development of the cascade to be seen. Little development of the cascade takes place in the gas but it allows a snapshot of how the particle number increases, and then decreases, as the shower progresses through more and more lead. Each lead plate (the dark bands running horizontally across the picture) is about two radiation lengths thick and the area of the picture is 0.5 m $\times$ 0.3 m. The features in this picture, except for scale, are extremely similar to those present when a high-energy particle enters the earth's atmosphere and creates an air shower. All of the important features of shower development, such as the rise and fall of the particle numbers, and the lateral spreading of the shower, are evident, as are some muons that penetrate much deeper in the chamber than most of the electrons.

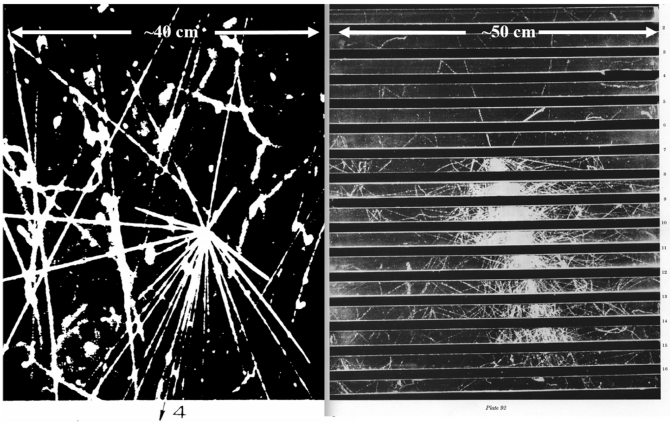

Fig. 1. Left: Interaction of a proton with a nucleus of argon in a cloud chamber, filled with argon at 70 atmospheres, operated at 3343 m. Right: Development of a shower in a multi-plate cloud chamber operated at 3230 m. For further details, see the text.

The incoming particle can be identified as a proton with some confidence. The level of ionisation excludes a heavier nucleus and the traversal of the particle through six lead plates (about 88.5 $\mathrm{g\,cm^{-2}}$ or 13.9 radiation lengths) strongly excludes the possibility that the incoming particle is an electron. To have the point of interaction, presumably with a lead nucleus, in 7^{th} plate is very reasonable, as we now know that the p-air cross section at the energy in question ($\sim$ 10 GeV) is around 250 mb (equivalent to 80 $\mathrm{g\,cm^{-2}}$), and that the interaction length in lead is about 194 $\mathrm{g\,cm^{-2}}$. The interaction with one of the nucleons of lead can be represented as

$$p + p \to p + p + N\left(\pi^{+} + \pi^{-} + \pi^{0}\right) ,$$

where the first proton is the cosmic ray and the second proton is within the target nucleus. A very similar equation would correspond to the target nucleon being a neutron. Of course, charge and all the other familiar quantum numbers must be conserved. Here, and in what follows, I have ignored the presence of particles such as $K, \Lambda, \eta, \Omega, \Sigma \ldots$ which are undoubtedly created and which are treated correctly in detailed Monte Carlo calculations. Some of the discussion above requires an understanding of the development of air showers which I will now address. I will aim to clarify how the deductions about the particle initiation the cascade shown in Fig. 1 could be made.

The energy spectrum of cosmic rays, shown in Fig. 2, has now been measured to 100 EeV, with the air shower technique being the only method available above about 0.1 PeV.

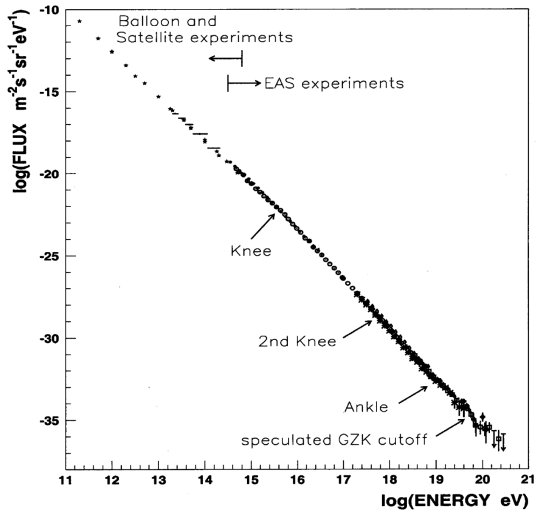

Fig. 2. Observed spectrum of primary cosmic rays. Various features are marked. The material of the present article is mainly concerned with the high-energy portion of the spectrum (after figure by S. Swordy).

3. The electromagnetic portion of the cascade

It is convenient to follow first the fate of the π^0s. At rest, these particles have a mean lifetime of 10^{-16} s and so, except at the most extreme energies, will nearly always decay. The most common decay mode is into two gamma rays, $\pi^0 \to \gamma\gamma$. The decays, $\pi^0 \to \gamma + e^+e^-$ and $\pi^0 \to e^+e^-e^+e^-$ are also possible, but can be ignored in a preliminary discussion. Photons, in the electric field of a nucleus of atomic number Z, will produce electron pairs with a mean free path

$$\lambda_{\rm pair} = 1/n\sigma_{\rm pair}\,,$$

where n is the number density of nuclei of atomic mass A of the material through which the photon is travelling. The cross section is given by

$$\sigma_{\rm pair} \cong \left(\left(Z^2 r_e^2\right)/137\right)(28/9)\ln\left(183/Z^{1/3}\right)\ {\rm cm}^2\,,$$

which, for air, reduces to

$$\sigma_{\rm pair} \cong 5.7 r_e^2 = 6 \times 10^{-26}\ {\rm cm}^2\,,$$

where r_e is the classical radius of the electron. Pair production is a catastrophic process for the photon. The electrons of the pair, however, produced with an opening angle $\theta \sim mc^2/h\nu$, go on to produce further photons through the process of bremsstrahlung. Here, $h\nu$ is the energy of the photon. Bremsstrahlung and pair production are very similar processes. Bremsstrahlung can be thought of classically as the radiation emitted when any charged particle, here an electron or positron, is accelerated in the field of a nucleus. The cross section for pair production, $\sigma_{\rm pair}$, and the cross section for bremsstrahlung, $\sigma_{\rm brem}$, are simply related by

$$\sigma_{\rm pair} = (7/9)\sigma_{\rm brem}$$

which reflects the similarity of the two processes at the quantum-mechanical level. The spectrum of photons emitted in the bremsstrahlung process is a flat one with, to a reasonable approximation, all energies up to the energy of the electron itself being emitted with equal probability. The root-mean-square angle of emission is $\sim mc^2/E$, where E is the energy of the radiated photon. Thus, low-energy photons can be emitted at large angles.

Energy loss by an electron is a stochastic process and it is convenient to characterise it in terms of the radiation length, X_0, where the energy, E, retained by an electron is given by

$$E = E_0 \exp(-x/X_0)\,,$$

with E_0 being the energy of the electron as it starts to traverse material of thickness x. Note that for bremsstrahlung the energy loss, $-\mathrm{d}E/\mathrm{d}x$, is proportional to E and is the most important source of loss other than ionisation at energies above about 10 MeV. However, as the electron loses energy, there comes a point at which the rate of energy loss due to bremsstrahlung falls below the rate of energy loss due to ionisation. When

$$-\mathrm{d}E/\mathrm{d}x|_{\mathrm{brem}} = -\mathrm{d}E/\mathrm{d}x|_{\mathrm{ionisation}}\,,$$

the electron is said to be at the critical energy, $E = \varepsilon_{\mathrm{c}}$. In air, this is about 84 MeV.

A helpful insight into the development of an electromagnetic cascade was given many years ago by Heitler [2] through a 'Toy Model' (see Fig. 3, left-hand diagram). Assume that after a distance λ, taken as equal to the mean free path for pair production, an electron pair is created with each electron taking half of the initial energy, E_0. Approximating the mean free path for bremsstrahlung as equal to that for pair production (*i.e.* ignoring the factor 7/9), we can assume that a bremsstrahlung process takes place for each electron after a further distance, λ. The cascade, continues with the energy being shared equally at each branching node, until that rate of energy loss by bremsstrahlung equals the rate of energy loss by ionisation, *i.e.* until the electron energy has fallen to ε_{c}. Suppose that this happens after a depth X, then the number of branching nodes, $n = X/\lambda$. Hence, the number of track segments of electrons and photons at a depth X is given by

$$N(X) = 2^{X/\lambda}\,.$$

The energy of the electrons and photons has degraded to $E(X) = E_0/N(X)$ at depth X. Hence, the number of particles at shower maximum (electrons and photons) is $N(X_{\mathrm{max}}) = E_0/\varepsilon_{\mathrm{c}}$ and the depth at which the shower reaches maximum is given by

$$X_{\mathrm{max}} = \lambda \ln(E_0/\varepsilon_{\mathrm{c}})/\ln 2\,.$$

This last relation is a useful descriptor of how the depth of shower maximum changes with energy

$$\mathrm{d}X_{\mathrm{max}}/\mathrm{d}E_0\,,$$

the 'elongation rate' and is useful in discussion of mass composition (see below). These ideas can be used to make a very crude estimate of the energy of the particle that initiates the cascade in the right-hand picture in Fig. 1: it is around 10 GeV.

The above paragraphs give some basic details about the development of the electromagnetic cascade. The processes of bremsstrahlung and pair production are extremely well-understood and all cross sections are accurately calculable from theory based on quantum electrodynamics (QED). In the 1950s and 1960s, extensive analytical calculations were developed, particularly by Nishimura and Kamata in Japan, to describe electromagnetic cascades and these were followed by Monte Carlo calculations which allow the cascades to be examined in further detail.

4. The hadronic portion of the cascade

In extensive air showers initiated by protons or nuclei, the hadronic part of the cascade is crucial to feeding the electromagnetic cascade but its development is much harder to describe in a simple manner as the details of key parameters, such as cross section, inelasticity and multiplicity, are poorly known from experiment and cannot yet be calculated from theory. In particular, of course, the energies of interest in the earliest stages of the development of air showers are well-beyond accelerator energies and one has to remain alert for surprises. For example, up until the discovery of the rise in the cross section of proton–proton interactions in 1973, it had been widely believed that the cross section had reached an asymptotic limit that would remain to the very highest energies. Similarly, the ideas of Feynman concerning the 'scaling' of inclusive cross sections led to predictions about the variation of multiplicity of secondary particles produced in collisions, at variance with what was later found by experiment. We thus have a much more tenuous grasp on several key aspects of shower development than is desirable.

An insightful analysis, similar to that given by Heitler, has been developed for the hadronic cascade by Matthews [3]. His approach is shown alongside that of Heitler for the electromagnetic case in Fig. 3.

In Matthews's approach, the $\pi^{+/-}$s and π^0s emerge from the first collision. The neutral pions decay to photons almost immediately and their progress can be tracked as in the left-hand figure. The charged pions travel some distance and then interact to produce a new generation of pions of all types. This multiplication continues until the individual pion energies drop below a critical energy, ξ_c^π, where decay becomes more likely than interaction. The critical energy is around 20 GeV in air. At this point in the development, all charged pions are assumed to decay into muons which are propagated to the ground without energy loss or decay. In a first approximation, it is assumed that the interactions are perfectly inelastic with all of the energy going into new particles although in [3], a deeper analysis is additionally presented that includes a leading particle which carries away a significant portion of the energy.

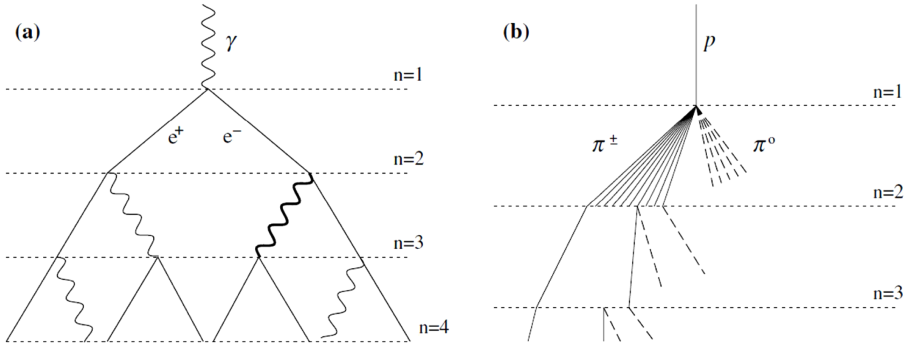

Fig. 3. Schematic views of (a) an electromagnetic cascade and (b) a hadronic shower. In the hadron shower, dashed lines indicate neutral pions which do not interact, but quickly decay, yielding electromagnetic sub-showers (not shown). Not all pion lines are shown after the $n = 2$ level. Neither diagram is to scale: taken from [3].

In the case of proton or pion interaction, the analysis assumes that a leading nucleon takes away more of the energy than any other particle created. The inelasticity, κ, is not a fixed quantity but can vary between 0 and 1. It can be useful for rough estimates to take $\kappa = 0.5$, so that half of the energy is transferred to pions, but this is a crude approximation. Charge independence dictates that energy is shared equally between the three sets of pions: thus in a collision of a leading nucleon approximately $0.5 \times 0.33 = 0.16$ of the energy of the leading nucleon transfers, through the neutral pions, to the electromagnetic cascade. As an example, following [3], consider a single proton entering the atmosphere with an energy, E. After n interaction layers, there are $N_\pi = (N_{\rm ch})^n$ total charged particles, and, assuming the equal division of energy during production, these particles carry a total energy of $(2/3)^n E$. The energy per pion is thus $E_\pi = E/(2N_{\rm ch}/3)^n$.

It is a useful to study the approach of [3] and to realise how these simple ideas lead to an understanding of how an air shower develops. A simple conclusion is that much of the energy is carried by the electromagnetic cascade. Additionally, the manner in which the depth of shower maximum, $X_{\rm max}$, changes with energy gives an important clue to the primary mass as we will see later. The muon number that is observed is also dependent on the primary mass. This latter point is very important although it is costly to measure muons because of the shielding needed to isolate them from the electromagnetic component. As shown in [3], the number of muons in a shower produced by a primary of mass A, assuming the interaction of a nucleus with mass A behaves as the interaction of A nucleons, each of energy E/A, is given by $N_\mu^p A^{0.15}$, where N_μ^p is the number of muons found in a shower initiated by protons.

The different relative importance of neutral pions (and the resulting electromagnetic cascade) and charged pions in the shower development process can be understood from the two diagrams in Fig. 4 which show the development of the electrons and muons, in terms of the energy deposited per $\mathrm{g\,cm^{-2}}$, for a shower produced by a proton of 10^{19} eV.

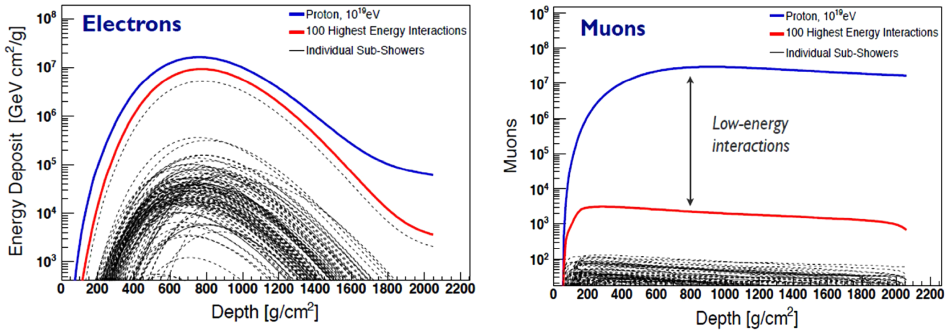

Fig. 4. (Colour on-line) These plots show the total number of electrons and muons as a function of atmospheric depth (1 atmosphere at sea level $\sim$ 1000 $\mathrm{g\,cm^{-2}}$). The solid black/blue curves show the total energy deposited (in GeV per $\mathrm{g\,cm^{-2}}$) in the atmosphere by electrons and muons. The solid gey/red curves are the sums from the 100 most energetic interactions that occur as the shower develops. Most of the electrons come from these 100 interactions, while the bulk of the muons come from energy interactions at around the critical energy of $\sim$ 20 GeV. These plots are taken from [4].

Note the clear maximum in the electromagnetic cascade and its relatively rapid decline. Contrast this with the broad development curve of the muons which lose energy only by ionisation.

5. Methods of shower detection

The evolution of methods to study extensive air showers has been considerable since their first detections with a few Geiger counters in the 1930s. As the lectures were focussed on the highest-energy cosmic rays, I will describe briefly only the two observatories that are currently producing all of the information about these particles. The exposures from these instruments exceeds the sum of all previous exposures by about an order of magnitude and so the earlier results can be ignored for many purposes.

At the Pierre Auger Observatory, 1600 water-Cherenkov detectors, each 1.2 m deep, of 10 $\mathrm{m^2}$ area and containing 12 tonnes of water, are deployed over 3000 $\mathrm{km^2}$. Fluorescence radiation, produced by particles in the shower exciting nitrogen in the volume of air above this area, is observed using 24 telescopes located at 4 stations on the perimeter of the array. The Observa-

tory is located near the city of Malargüe in Argentina at a latitude of 35.2°S with a mean atmospheric overburden of 875 $\mathrm{g\,cm^{-2}}$, 1300–1400 m above sea level. The surface array is operated with nearly 100% efficiency while the fluorescence detection takes place only during clear, moonless, nights. Data-taking began in January 2004 with the last tank deployed in June 2008: data-taking is on-going. A detailed description of the Observatory has been given recently in [5]. The combination of the operation of a particle detector and a fluorescence detector, the hybrid method, was pioneered by the Auger Collaboration. The Observatory, because of the depth of the water-Cherenkov detectors, is able to record useful numbers of events out to 80° from the zenith, thus covering the sky up to declinations of $\sim 44°$N.

The Telescope Array (TA) is constructed near the town of Delta, Utah, USA at a latitude of 39.3°N and at an altitude of 1400 m, very similar to that of the Auger Observatory. Thus, the two observatories cover the whole sky with an overlap in declination range $-15.7° < \delta < 25.5°$ within which useful flux comparisons can be made. The Telescope Array contains 507 scintillators, each of two layers, 3 $\mathrm{m^2}$ in area and 1.2 cm thick, arranged on a square lattice with a spacing of 1.2 km covering 680 $\mathrm{km^2}$. The Telescope Array also uses the hybrid method with complexes of 14, 12 and 12 fluorescence telescopes on promontories near the edges of the area. Detailed descriptions of the scintillator array and of the fluorescence detector complex of the Telescope Array can be found in [6] and [7].

Because of the longer operating time of the Auger Observatory and the larger aperture available with the deeper detectors, the Auger exposure (currently close to 80,000 $\mathrm{km^2\,sr\,yr}$) is about eight times that of the Telescope Array. Such enormous exposures are necessary as the rate of events above 5×10^{19} eV is only about 1 per $\mathrm{km^2}$ per century.

6. Experimental results

The 36$^{\mathrm{th}}$ Biennial International Cosmic Ray Conference (ICRC) was held in Madison, USA about a month after the Cracow School in Zakopane: the first ICRC was held in Cracow in 1947. The papers presented at this meeting are readily available from the Conference Web site and videos of reviews, highlight talks and rapporteur presentations are available at `www.icrc2019.org`. Highlight talks were given by Castellina [8] and Ogio [9] on behalf of the Auger and Telescope collaborations, respectively, and provide excellent guides to the present status of the field. The Rapporteur talk of F. Schroeder is also strongly recommended. In what follows, I will attempt to summarise the situation with regard to measurements of the energy spectrum, the arrival distributions and the mass composition of cosmic rays above $\sim 10^{18}$ eV, key areas of study from the viewpoint of discovering the origin of the highest energy particles.

7. The energy spectrum

The hybrid method of shower detection used by the Auger and Telescope collaborations enables the relatively high rate of events recorded with the surface detectors to be exploited. However, if one had only surface detectors, one would need to recourse to shower simulations, which involve input about hadronic interactions that remains uncertain at the energies in question, to estimate the primary energy. The approach to overcoming this issue is to calibrate the measurements made with the surface detectors with calorimetric estimates of the primary energy derived from the fluorescence observations. Typical calibration data are shown in Fig. 5.

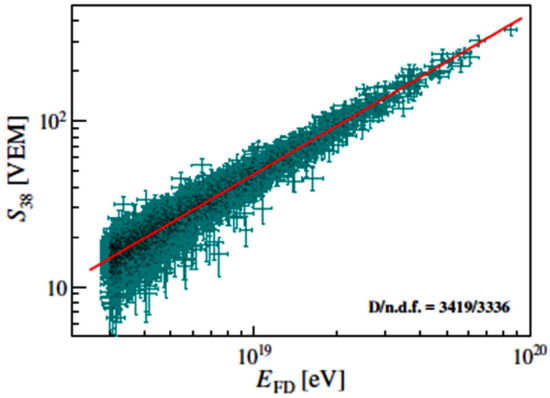

Fig. 5. Correlation between the energy estimator from the surface array of the Auger Observatory and the energy reconstructed using the fluorescence detector for 3338 'hybrid' events, see [10] for more details.

The energy spectrum from work with the Auger Observatory is shown in Fig. 6 where the spectrum shown is unfolded from the raw measurements by taking account of the energy resolution. In the right-hand plot, the differential intensity has been multiplied by E^3 so that features in the spectrum can be seen more clearly. In particular, a flattening of the spectrum, usually called 'the ankle', is evident at $\sim 5 \times 10^{18}$ eV and the spectrum steepens sharply about one decade higher. Before this, at $\sim 10^{19}$ eV, the spectrum steepens less sharply, a feature that is now reported for the first time. Implications of these results are discussed below. It cannot be stressed too strongly that the energy estimates are derived solely from the data and do not depend on assumptions about hadronic interactions. This approach differs from that of *all other* spectrum determinations (including that of the Telescope Array Collaboration) above $\sim 5 \times 10^{14}$ eV where the air-shower phenomenon is used.

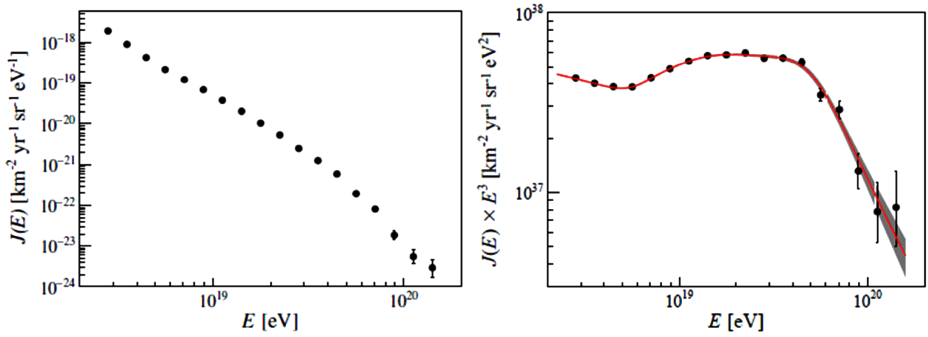

Fig. 6. The energy spectrum measured using data from the Pierre Auger Observatory. The spectrum is based on 215,030 events with over 1600 greater than 10^{19} eV. In the right-hand plot, the differential intensity, $J(E)$, has been multiplied by E^3 so that features in the spectrum are more readily seen [10].

The energy spectrum has been measured by the Telescope Array in a broadly similar manner, though with lower statistics and with input from shower simulations and assumptions about the primary mass. A comparison of the results is shown in Fig. 7.

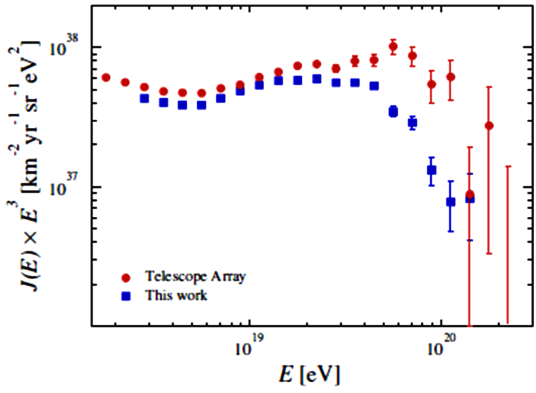

Fig. 7. Comparison of the results from the Auger Observatory [10] and those derived from the Telescope Array [9]. See [10] for further details.

It is clear that there are some differences between the two measurements. A useful place to make a comparison is at the position of the ankle. As there are no indications of anisotropies in arrival directions in either sets of data, this spectral feature is expected to be unchanged across the sky and so the observed fluxes should be identical. The ankle position, as measured by the Telescope Array, is at $(4.4 \pm 0.1$ (statistical) $\times\ 10^{18}$ eV; for the Auger Observatory the equivalent figure is $(5.2 \pm 0.1$ (statistical) $\pm$ 0.7 (system-

atic)) $\times$ 10^{18} eV. This is a difference of only 2.1 σ when considering only statistical uncertainties and in good agreement when systematic uncertainties are taken into account. Consistency in the ankle region can be obtained by rescaling energies by +5.2% for Auger and by −5.2% for TA. These factors are smaller than the systematic uncertainties in the energy scales estimated for each measurement which are about 21% (TA) and 14% (Auger).

However, even after these adjustments, significant differences persist above 10^{19} eV. At such high energies, it is not unreasonable to envision the possibility of different intensities in the Northern and Southern Hemispheres but before making such a claim, it is necessary to examine measurements from the portion of sky visible to both instruments. A further empirical systematic shift of +10% (−10%) per decade for Auger (TA) would be required to bring the spectra into agreement. A comprehensive search for such energy-dependent systematic uncertainties has been made by a joint Auger/TA working group but thus far the reason for the anomaly is not understood.

8. The arrival direction distributions

It has long been anticipated that at a sufficiently high energy, anisotropies in the arrival directions of cosmic rays might be observed. At low energies, these might be expected to arise from diffusion of particles in the magnetic fields of the galaxy, while at the highest energies, rectilinear propagation might dominate. At last, after decades of effort, convincing evidence of directional anisotropies is being obtained. Above 8×10^{18} eV, the Auger Observatory have detected evidence of a dipole, when the directions are considered in right ascension, that is significant at over $6\,\sigma$ [8, 11] and which may be correlated with the distribution of galaxies from the 2MRS (infra-

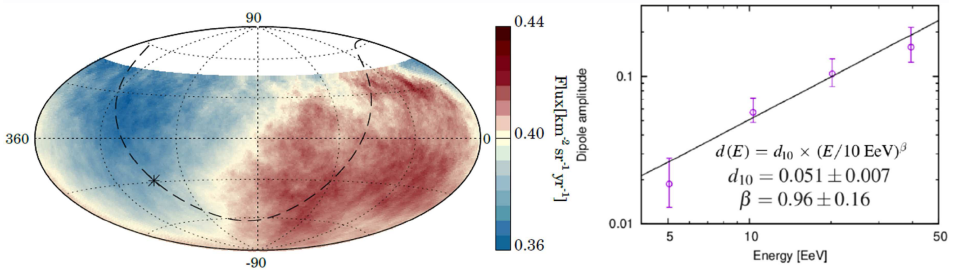

Fig. 8. Left (colour on-line): The cosmic ray flux, in equatorial coordinates (right ascension is plotted from right to left) above 8×10^{18} eV, averaged over top-hat windows of 45° radius. The galactic plane is shown by the dashed line with the Galactic Centre indicated by a star. Right: The energy dependence of the amplitude above 4×10^{18} eV.

red) survey. The amplitude of this anisotropy increases with energy [12] and its direction strongly suggests that these particles come from outside of our Galaxy. Although this is not a surprising conclusion because of our understanding of galactic magnetic fields and of potential sources within it, this is the first experimental evidence to support this hypothesis. The data are shown in Fig. 8.

At even higher energies, evidence for point sources is starting to emerge, see [8] for the latest details. A model-independent blind search for overdensities has been carried out across the whole field of view in the energy range of 3.2–8 $\times$ 10^{19} eV. The most significant excess, in an angular window of 27°, was found in the direction of $\alpha = 202°$ and $\delta = 45°$ with a post-trials significance of $3.9\,\sigma$. This region is densely populated with extragalactic objects including the closest radio galaxy, Centaurus A and a starburst galaxy, NGC 305.3. Although the angular resolution of the observatory is better than 1°, bending in intermediate magnetic fields makes a positive identification with either object difficult. Indeed both might be sources of UHECR.

The arrival directions of UHECRs detected by the Auger Observatory have also been compared with the distribution of nearby extragalactic matter in four catalogues:

(a) a sample of 32 starburst galaxies (SBGs) selected based on their continuum emission at 1.4 GHz, used as a proxy for their UHECR flux;

(b) a selection of γAGNs from the 3FHL catalogue, weighting the sources with the integral flux from 10 GeV to 1 TeV;

(c) the 2MRS catalogue of nearby matter farther than 1 Mpc;

(d) a selection of Swift-BAT radio-loud and radio-quiet AGNs.

In these analyses, the source directions, and also the relative UHECR fluxes from source candidates provided by the observations from Fermi-LAT, were used together with knowledge of the mass composition (see below) to allow an evaluation of the attenuation of intensity caused by energy losses during propagation. Our current knowledge of the cosmic-ray mass-composition was used in this evaluation. A likelihood-ratio analysis was adopted to evaluate the smearing angle and the fraction of anisotropic cosmic rays for each catalogue. The test statistics obtained for the correlation with SBGs and γAGNs is shown in the left panel of Fig. 9. The highest significance is obtained for the case of SBGs with an anisotropic fraction of $(11 \pm 5)\%$ of events with energy above 3.8 $\times$ 10^{19} eV in a smearing angle of 15°. After penalization for the scanning in energy, the significance of the correlation is found to be $4.5\,\sigma$. The cumulated test statistics for $E_{\rm thr} = 3.8 \times 10^{19}$ eV

(Auger scale) is shown in the right panel of Fig. 9 as a function of the number of events recorded. A growth of the significance since the first report [13] in 2018 until the report at the recent International Cosmic Ray Conference (2019) is evident: ~ 250 events have been added, $\sim$ 10% of the total.

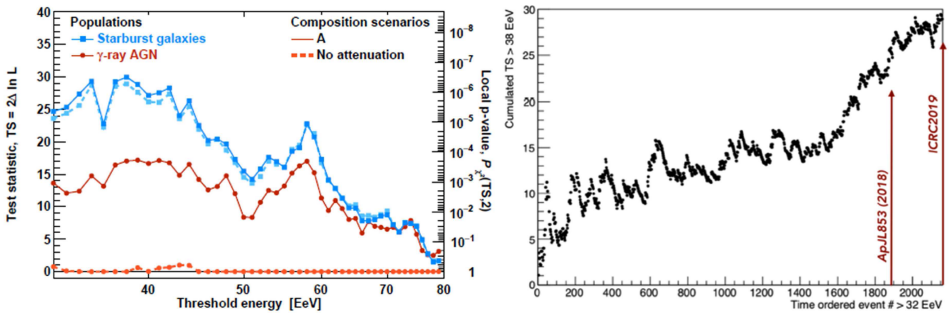

Fig. 9. Left: Maximum likelihood ratio as a function of energy for the startburst galaxy and γAGN modes. Cumulative test statistic for an energy threshold for 38 EeV as a function of event number arranged in order of time of arrival. The level of significance at the time of publication has been surpassed with the addition of more data.

In 2008, the TA Collaboration first reported a broad 'hot spot' of radius 25° in the Northern Hemisphere from a study of events with $E > 5.7 \times 10^{19}$ eV (TA energy scale). The region is centred on $\alpha = 144.3°$, $\delta = 40.3°$ which is $\sim 20°$ from the supergalactic plane and not visible from the latitude of the Auger Observatory. After 5 years, the significance had reached $3.4\,\sigma$ after trials. After 11 years, this has fallen to $2.9\,\sigma$ [9]. The 'hot spot' is not associated with any object showing strong activity.

9. The mass composition

Determining the mass composition is more challenging than measuring the energy spectrum or the distribution of arrival directions. Currently, the most promising approach is to compare the change of the depth of shower maximum with energy, $X_{\max}$, (the elongation rate) with the predictions of models. Any inferences drawn are compromised by the lack of certainty over which model to use, with the additional possibility that none of the available options actually represents reality. The $X_{\max}$ measurements are made using the fluorescence detectors operated at the Auger and TA observatories. Again, the data set from the Auger Observatory is the more extensive but limited in the highest energy that can be reached with a reasonable statistical sample because of restricted on-time of the detectors. However, using the risetimes of signals in the large-area water-Cherenkov detectors,

calibrated with fluorescence-detector measurements, it has been possible to extend estimates to the highest energies. Additionally, for the direct measurements with the fluorescence detectors, the root-mean-square spread of $X_{\max}$ can be compared with predictions. Data from the Auger Observatory are shown in Fig. 10 together with comparison with predictions made using various models based on LHC information are shown. The measurement is based on 47,000 hybrid events of which ~ 1000 have energies above 10 EeV. The manner of the evolution of $\sigma(X_{\max})$ at the highest energies suggests a pure and heavy composition, while at lower energies, the results are compatible with a light or mixed composition. The two moments of the $X_{\max}$ distributions can be converted to $\ln A$, the logarithmic primary mass, and at 2×10^{18} eV, where there is evidence of a break in the elongation rate, $\ln A = 0.8$ (EPOS-LHC) and 1.4 (Sibyll 2.3c), while the values of $\sigma^2(\ln A)$ for QGSJetII-04 are unphysical, suggesting that this model should not be used to describe the Auger data.

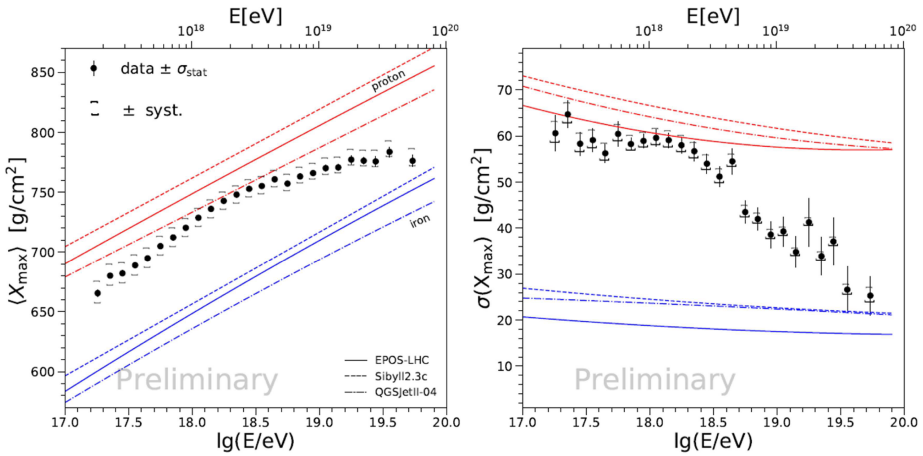

Fig. 10. The evolution of $X_{\max}$ and $\sigma(X_{\max})$ with energy compared with predictions from models that are based on LHC data.

The TA data set is more limited [14] with only 19 events above 1.2×10^{19} eV and comparisons that they have made is with predictions from the QGSjet suite of models that are disfavoured by the Auger data. At lower energies, it is claimed that the TA results are consistent with a composition comprising largely protons and helium. Although not noted by the TA Collaboration, an independent analysis suggests that there is a break in the elongation rate in their measurements at an energy not dissimilar to the position of that found in the Auger observations [15].

10. Interpretation of the data

A steepening in the energy spectrum of cosmic rays above $\sim 5 \times 10^{19}$ has now been observed. This had long been anticipated following the predictions of Greisen and Zatsepin and Kuz'min [16, 17]. However, now that a steepening has, without question, been seen by the HiRes, Auger and TA collaborations, it is becoming increasingly clear that an alternative explanation in terms of models in which the maximum energy reached by acceleration is proportional to Z, the charge of the nucleus accelerated, appears attractive. Some of these models predict something like the observed mass distribution in a natural manner.

In one model [18], it is assumed that identical sources are distributed in a co-moving volume, with the nuclei accelerated through a rigidity-dependent mechanism. The fit to the latest data (Fig. 11) suggests sources characterised by relatively low maximum injection energies, hard spectra and a heavy mass composition. This model [18] does not match the measured spectrum at energies below about 5×10^{18} eV. Other models [19, 20] have been developed with more attention given to the acceleration regions and these are able to fit the spectrum to 10^{18} eV (Fig. 12). A further appealing feature of [19, 20] is that these models provide a natural explanation for the observed dominance of protons near 10^{18} eV and the low level of anisotropy, features counter to what might be expected if particles of this energy were dominantly galactic. These protons arise from the decay of neutrons produced in the sources as a result of photodisintegration.

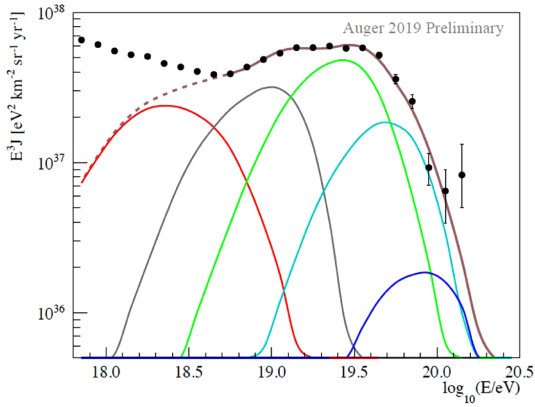

Fig. 11. (Colour on-line) The simulated energy spectrum (multiplied by E^3) is obtained with best fit parameters: atmosphere: all-particle (upper/brown curve) and from left to right: $A = 1$ (red), $2 < A < 4$ (grey), $5 < A < 22$ (green), $23 < A < 38$ (cyan), $A < 39$ (blue). The spectrum from the right-hand plot in Fig. 6 is shown by the black dots [18].

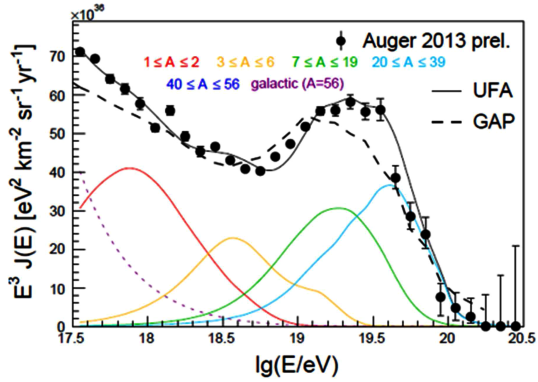

Fig. 12. (Colour on-line) The extragalactic cosmic ray fluxes as a function of energy for protons, helium and a range of different nuclei fitted to an earlier version of the Auger energy spectrum. UFA refers to the work of Unger *et al.* [19], while GAP relates that of Globus *et al.* [20].

In the energy range where UHECRs are of extra-galactic origin, the measurements lead to an energy density filling factor of the Universe in cosmic rays. To supply this energy to every volume element of the Universe during the accumulation time of UHECRs, which is limited by energy losses, the accelerators considered in the benchmark scenario must dump into extra-galactic space a power density in cosmic rays of $\approx 5 \times 10^{44}$ erg Mpc^{-3} yr^{-1} above 5×10^{18} eV. Only a handful of astrophysical sites produce such a power in non-thermal photon radiation.

11. Future projects

For the next phase of the study of these high-energy particles, both the Auger and Telescope Array collaborations are moving forward with funded plans. The Telescope Array will expand the area of their surface array by a factor of four, making it nearly as large as the Auger Observatory: the primary physics goal is the study of the 'hot spot' identified by them some years ago in more detail [9]. The Auger Collaboration are deploying 4 m^2 scintillators on top of each of the 1600 water-Cherenkov detectors and, in addition, are adding radio antenna at every station. The goal is to identify the mass of primary particles on an event-by-event basis with the objective of enhancing anisotropy studies [8].

There are more ambitious plans to achieve much larger exposures, one of which was conceived by John Linsley in the late 1970s. His vision was to deploy a fluorescence detector in space. A proposal to ESA to fly a single fluorescence detector on the International Space Station was developed by Linsley, with L. Scarsi and Y. Takahashi as collaborators, under the

name EUSO (Extreme Universe Space Observatory). Despite an impressive phase A study, ESA funding problems led to the project being dropped later to emerge as JEM-EUSO with plans to mount such a device in the Japanese module on the Space Station. This plan also foundered but the EUSO concept remains very much alive with a mini-EUSO now docked on the Space Station and observations scheduled to start with the arrival of trained astronauts in October 2019. This mission is one of several that are part of the program behind the POEMMA (Probe of Extreme Multi-messenger Astrophysics) project, a twin-satellite mission that is being developed for launch by NASA.

The promise of POEMMA is to open two cosmic windows. One will allow the search for neutrinos above 20 PeV by looking for showers generated by tau-neutrinos as they exit the earth. The other is the study of UHECR above 30 EeV. POEMMA is planned to have an exposure one order of magnitude larger than achieved hitherto, with the prospect of rewriting 'the textbook on the most extreme astrophysical accelerators and fundamental physics interactions above terrestrial accelerator energies'. Launch is planned for the late 2020s.

A successful POEMMA mission will surely require a follow-up on the ground. I have likened this to the construction of LEP which was to enable high-precision studies of the Z and W particles discovered at the SPS. To cover $\sim$ 30,000 km^2 will require cheaper technologies: water-Cherenkov detectors will surely remain the workhorse of the installation, and can probably be made more cheaply, while an inexpensive fluorescence detector, FAST, is being developed [21].

This giant array should have the fluorescence detectors spaced sufficiently close to cover the whole area with a sensitivity to energies as low as 0.5 EeV. This would allow a search for the two showers expected to arrive simultaneously as a consequence of photo-disintegration of a nucleus in the solar photon field. This idea was proposed by Zatsepin and developed further by Gerasimova and Zatsepin [22] in the 1950s. Taking ^{12}C as an example, the showers produced by a neutron and ^{11}C would differ by a factor of 11 in energy and so, in principle, the mass of the primary could be found rather directly. There seems no prospect of making such an observation with particle detectors as the showers produced by the neutron and the ^{11}C nucleus would require an impractically-dense spacing of detectors to measure them. In the earliest considerations, the deflection of the charged fragments in the interplanetary magnetic field was overlooked, but this was taken into account in later work [23, 24]. For an iron primary [23], the separation of the showers is generally too large even for the size of array envisaged here, but for lighter primaries, it has been shown that separations of only a 100 km or so are expected [24].

The approach proposed for a giant ground-based detector is a combination of brute force and elegance, the latter lying in the prospect of a direct measurement of the primary mass. Such an achievement would be hugely significant: in addition to its implications for cosmic-ray research, it would open the prospect of testing models of hadronic interactions rather directly at energies well-beyond what is possible at the LHC.

The high-energy cosmic-ray field is more vibrant that it has ever been with a very bright future and I can only envy those young enough to enjoy it.

My grateful thanks go to Michał Praszałowicz for inviting me to lecture at the Cracow School, to my Auger colleagues for continuing stimulation and to Antonella Castellina for her very clear highlight talk at the recent ICRC in Madison from which I have borrowed some diagrams quite shamelessly!

REFERENCES

[1] K.-H. Kampert, A.A. Watson, *Eur. Phys. J. H* **37**, 359 (2012) [arXiv:1207.4827 [physics.hist-ph]].

[2] W. Heitler, *The Quantum Theory of Radiation*, 3rd edition, Oxford University Press, London 1954, p. 386.

[3] J. Matthews, *Astropart. Phys.* **22**, 387 (2005).

[4] R. Ulrich, C. Baus, R. Engel, *EPJ Web Conf.* **99**, 11001 (2015).

[5] Pierre Auger Collaboration, *Nucl. Instrum. Methods Phys. Res. A* **798**, 172 (2015).

[6] Telescope Array Collaboration, *Nucl. Instrum Methods Phys. Res. A* **689**, 87 (2012) [arXiv:1201.4964 [astro-ph.IM]].

[7] H. Tokuno *et al.*, *Nucl. Instrum Methods Phys. Res. A* **676**, 54 (2012).

[8] A. Castellina, *PoS* **(ICRC2019)**, 004 (2019).

[9] S. Ogio, *PoS* **(ICRC2019)**, 013 (2019).

[10] Pierre Auger Collaboration, A Measurement of the Cosmic Ray Energy Spectrum Above 2.5×10^{18} eV Using the Pierre Auger Observatory, submitted to *Phys. Rev. D.*

[11] Pierre Auger Collaboration, *Science* **357**, 1266 (2017).

[12] Pierre Auger Collaboration, *Astrophys. J.* **868**, 4 (2018).

[13] Pierre Auger Collaboration, *Astrophys. J. Lett.* **853**, L29 (2018).

[14] W. Hanlon, *PoS* **(ICRC2019)**, 280 (2019).

[15] A.A. Watson, *EPJ Web Conf.* **210**, 00001 (2018).

[16] K. Greisen, *Phys. Rev. Lett.* **16**, 748 (1966).

[17] G.T. Zatsepin, V.A. Kuz'min, *JETP Lett.* **4**, 78 (1966).

[18] Pierre Auger Collaboration, *J. Cosmol. Astropart. Phys.* **04**, 038 (2017) [*Erratum ibid.* **03**, E02 (2018)].

[19] M. Unger, G. Farrar, L. Anchordoqui, *Phys. Rev. D* **92**, 123001 (2015) [arXiv:1505.02153 [astro-ph.HE]].

[20] N. Globus, D. Allard, E. Parizot, *Phys. Rev. D* **92**, 021302(R) (2015); L.V. Skripnikov *et al.*, *Phys. Rev. A* **92**, 032508 (2015) [arXiv:1505.0137 [physics.atom-ph]].

[21] T. Fuji *et al.*, *PoS* **(ICRC2019)**, 259 (2019).

[22] G.T. Zatsepin, *Dokl. Akad. Nauk SSSR* **80**, 577 (1951); N.M. Gerasimova, G.T. Zatsepin, *Sov. Phys.* **11**, 899 (1960).

[23] G. Medina Tanco, A.A. Watson, *Astropart. Phys.* **10**, 157 (1999).

[24] L. Epele, S. Mollerach, E. Roulet, *J. High Energy Phys.* **9903**, 017 (1999).